The Clouds of Venus: II. An Investigation of the Influence of Coagulation on the Observed Droplet Size Distribution[1]

WILLIAM B. ROSSOW

Geophysical Fluid Dynamics Program, Princeton University, Princeton, N.J. 08540

(Manuscript received 5 March 1976, in revised form 30 August 1976)

ABSTRACT

Using an approximate numerical technique, we investigate the influence of coagulation, sedimentation and turbulent motions on the observed droplet size distribution in the upper layers of the Venus clouds. If the cloud mass mixing ratio is $<10^{-6}$ at 250 K or the eddy diffusivity throughout the cloud is $>10^6$ cm^2 s^{-1}, then coagulation is unimportant. In this case, the observed droplet size distribution is the initial size distribution produced by the condensation of the droplets. We find that all cloud models with droplet formation near the cloud top (e.g., a photochemical model) must produce the observed droplet size distribution by condensation without subsequent modification by coagulation. We find, however, that neither meteoritic or surface dust can supply sufficient nucleating particles to account for the observed droplet number density. If, on the other hand, the cloud droplets are formed near the cloud bottom, the observed droplet size distribution can be produced solely by the interaction of coagulation and dynamics; all information about the initial size distribution is lost. The eddy diffusivity is $\sim 5\times 10^5$ cm^2 s^{-1}. If droplet formation occurs near the cloud bottom, then the lower atmosphere of Venus is oxidizing rather than reducing.

1. Introduction

The only clues to the structure of the extensive cloud system on Venus come from the properties of the topmost layers. The particles near the 50 mb pressure level are liquid droplets with a narrow size distribution about a mean effective radius of 1.05 ± 0.1 μm (Hansen and Hovenier, 1974) composed of a 75–85% concentrated sulfuric acid solution in water (Young, 1973, 1975; Pollack *et al.*, 1975). The mass mixing ratio at different pressure levels has been inferred from observations at different wavelengths: $\sim 2\times 10^{-7}$ near 5–10 mb (Goody, 1967; O'Leary, 1975) from ultraviolet and visible wavelength observations of the limb, $\sim 10^{-6}$ near 50 mb (Hansen and Hovenier, 1974) from visible wavelength polarization measurements, $\sim 2\times 10^{-6}$ near 200 mb (Regas *et al.*, 1972, 1975) from near-infrared absorption line measurements, and $\sim 5\times 10^{-6}$ near 300 mb (Samuelson *et al.*, 1975) from infrared observations. These values are consistent with the microwave upper limit of $\sim 10^{-5}$ (Rossow and Sagan, 1975). Lateral homogeneity was demonstrated by the thermal infrared emission maps analyzed by Ingersoll and Orton (1974), while Mariner 10 limb photographs showed vertical inhomogeneity in the form of thin, detached haze layers near the cloud top.

These observations do not yet define uniquely the structure of the top layers of the cloud. In this paper we investigate the interaction of atmospheric dynamic motions and cloud microphysics in order to learn what role this interaction plays in determining the structure of the upper cloud layers. Specifically we are interested in whether or not this interaction can produce an upper layer of nearly uniform size droplets of 1 μm radius.

The physical processes which can influence the cloud structure are winds, sedimentation, collisions between droplets, and condensation or evaporation of the droplets. Unlike water droplets on Earth, the evaporation and condensation of the cloud droplets on Venus involves two vapors, water and sulfuric acid. Since the equilibrium vapor pressure of sulfuric acid over the droplets is an extremely strong function of temperature, we argue in Section 2 that the formation and destruction of the droplets involving the active condensation or evaporation of sulfuric acid vapor occurs only in two localized regions of small vertical extent. Throughout the bulk of the Venus clouds, then, water is the only active vapor, condensing and evaporating to maintain equilibrium composition of the droplet at all levels (Young, 1973; Rossow and Sagan, 1975). However, for these highly concentrated solutions, the mass increase due to condensing water is only $\sim 25\%$ and can be neglected. Since the equilibrium vapor pressure of water over the droplets is

[1] Work begun while the author was at the Laboratory for Planetary Studies, Cornell University.

such a strong function of composition, the droplets are stabilized against vapor exchange. Thus, except for the small formation and destruction regions of the cloud, the droplets of sulfuric acid can be considered condensationally inactive.

Of the two collisional growth processes, gravitational coalescence and Brownian coagulation, the former process is inefficient for droplets <10 μm in radius because the hydrodynamic forces exerted by gas flow past them prevent collisions (Klett and Davis, 1973). Therefore, Brownian coagulation is probably the only microphysical process which can influence the droplets once they have formed. The structure of these clouds can then be determined by accounting for the effects of coagulation, sedimentation and atmospheric motions, with the condensation and evaporation regions acting as a source and sink of particles.

Assuming no mean winds and horizontal homogeneity, and parameterizing the time-variable winds by an eddy diffusivity parameter E, we can write the equation for the time rate of change of the droplet number mixing ratio $q(m,z,t)$ as a function of droplet mass and altitude as

$$\rho\frac{\partial q(m,z,t)}{\partial t}=\frac{1}{2}\rho^2\int_0^m K(m', m-m', z)q(m',z,t)\times q(m-m', z, t)dm'-\rho^2 q(m,z,t)\int_0^\infty K(m,m',z)\times q(m',z,t)dm'+\frac{\partial}{\partial z}\left[\rho E\frac{\partial q(m,z,t)}{\partial z}+\rho V_s q(m,z,t)\right]+S(m,z), \quad (1)$$

where $q(m,z,t)$ is the number of droplets per gram of atmosphere per mass interval at time t, ρ is the atmospheric density, V_s the sedimentation velocity and $K(m,m',z)$ the coagulation rate coefficient.

The first two terms in Eq. (1) represent the creation and destruction of droplets by coagulation. The next term represents the transport of droplets into and out of a volume element by eddy motions and sedimentation. We model condensation of the cloud droplets by the constant source term $S(m,z)$, while destruction of the droplets implies a lower boundary condition. Rossow and Gierasch (1977) (hereafter Paper I) have shown that, under Venus conditions, qualitatively correct and reasonably accurate approximate solutions to (1) for $\partial q/\partial t=0$ may be obtained in terms of the first three moments of the size distribution, χ_0, χ_1 and χ_2. They replace Eq. (1) by the following system of equations:

$$\left.\begin{aligned}&\left\{\frac{\partial}{\partial z}\left[\rho E\frac{\partial}{\partial z}+\tfrac{1}{2}\rho c\langle m\rangle^{\frac{1}{3}}+\rho c'\langle m\rangle^{\frac{1}{3}}\right]-\tfrac{1}{2}\rho^2 K_0\chi_0\right\}\chi_0+\left\{\frac{\partial}{\partial z}\left[\tfrac{1}{2}\rho c\langle m\rangle^{-\frac{1}{3}}\right]\right\}\chi_1=0\\&\left\{\frac{\partial}{\partial z}\left[\rho E\frac{\partial}{\partial z}+\tfrac{1}{2}\rho c\langle m\rangle^{\frac{1}{3}}+\rho c'\langle m\rangle^{\frac{1}{3}}\right]\right\}\chi_1+\left\{\frac{\partial}{\partial z}\left[\tfrac{1}{2}\rho c\langle m\rangle^{-\frac{1}{3}}\right]\right\}\chi_2=0\\&\left\{\frac{\partial}{\partial z}\left[\rho E\frac{\partial}{\partial z}+f_1\rho c\langle m\rangle^{\frac{1}{3}}+\rho c'\langle m\rangle^{\frac{1}{3}}\right]\right\}\chi_2+\rho^2 K_0\chi_1^2=0\end{aligned}\right\}, \quad (2)$$

where $K_0=8kT/3\eta$, k is Boltzmann's constant, T the absolute temperature, η the dynamic viscosity of the temperature, and

$$c=\frac{2\rho_p g}{9\eta}\left(\frac{4\pi\rho_x}{3}\right)^{-\frac{1}{3}}, \quad (3)$$

$$c'=\left(\frac{4\pi\rho_p}{3}\right)^{\frac{1}{3}}\beta c\lambda, \quad (4)$$

$$\langle m\rangle=\frac{\chi_1}{\chi_0}, \quad (5)$$

where ρ_p is the density of a droplet, g the acceleration of gravity, λ the gas mean free path and β the Cunningham factor.

We use Eqs. (2)–(5), together with the boundary conditions outlined in the next section, to investigate two general models of the effect of dynamics and microphysics on the cloud structure. The two models are as follows:

1) The number of droplets formed is controlled by the supply of dust to the formation level. The grains act as nucleating centers and the size of the droplets is controlled by the steady-state mass flux through the cloud (Model I).

2) The number of droplets is controlled by the interaction of coagulation with transport by dynamic motions and sedimentation (Model II).

The first model assumes that, for a cloud of fixed mass, the number of cloud droplets is governed by the number of nucleation centers supplied to the level where the cloud droplets are formed. The source of dust is assumed to be meteoritic dust, but we also investigate the contribution of dust from the surface of Venus. The second model assumes that the number of cloud droplets is governed by a balance between coagulation and transport. That is, coagulation reduces

the number of droplets until the coagulation time is of the order of the lifetime of a droplet in the cloud which is controlled by transport rates. The size of the droplets in both cloud models is then given by the mass of the cloud.

The boundary conditions to Eq. (2) for each of the cloud models are presented in Section 2. The general behavior of the solutions is illustrated and discussed in Section 3, while in Section 4 the results of the calculations are presented. Finally, in Section 5 we summarize our conclusions.

2. Boundary conditions

There are four levels of interest in the atmosphere-cloud system:

1) The top of the model atmosphere.
2) The droplet pyrolysis level (PL).
3) The droplet formation level (FL).
4) The planetary surface.

a. The top

In Model I, we must find a solution to (2) for the meteoritic dust as well as for the cloud droplets. The source of dust is assumed to be a constant flux of particles F_0, of mass m_0, into the top of the model atmosphere well above the visible cloud tops. The magnitude of F_0 is discussed in Paper I and is certainly $\lesssim 1$ cm^{-2} s^{-1} for 0.1 μm particles.

For the cloud droplets, we assume that the formation level is below the top of our model atmosphere. Therefore the boundary condition on the cloud droplets at the top is that the net downward flux is zero.

The top boundary condition is written

$$\left.\begin{aligned}
&\left[\rho E\frac{\partial}{\partial z}+\tfrac{1}{2}\rho c\langle m\rangle^{\frac{2}{3}}+\rho c'\langle m\rangle^{\frac{1}{3}}\right]\chi_0 \\
&\qquad +\tfrac{1}{2}\rho c\langle m\rangle^{-\frac{1}{3}}\chi_1=F_0 \\
&\left[\rho E\frac{\partial}{\partial z}+\tfrac{1}{2}\rho c\langle m\rangle^{\frac{2}{3}}+\rho c'\langle m\rangle^{\frac{1}{3}}\right]\chi_1 \\
&\qquad +\tfrac{1}{2}\rho c\langle m\rangle^{-\frac{1}{3}}\chi_2=F_0 m_0 \\
&\left[\rho E\frac{\partial}{\partial z}+f_1\rho c\langle m\rangle^{\frac{2}{3}}+\rho c'\langle m\rangle^{\frac{1}{3}}\right]\chi_2=F_0(m_0)^2
\end{aligned}\right\}, \quad (6)$$

where $F_0=0$ for cloud droplets and m_0 for dust grains assumes a radius of 0.1 μm and a density of 2 g cm^{-3}.

b. Droplet pyrolysis level (PL)

The evaporation of a sulfuric acid droplet is a sensitive function of the abundance of water in the atmosphere. Heating an aqueous solution of sulfuric acid and water drives off primarily water vapor forcing the droplets toward higher concentrations until the ratio of water to sulfuric acid in the vapor at equilibrium is equal to the total abundance ratio of water to sulfuric acid. Sulfuric acid vapor appears in abundance in the vapor only very near the evaporation temperature.

The location of the pyrolysis level can be estimated given the abundances of sulfuric acid and water in the atmosphere. Arguing from inferred cloud-top masses and the optical properties of the droplets, Young (1973) derives both a "wet" cloud with its bottom near 26 km altitude and a "dry" cloud with its bottom near 45 km altitude consistent with observations. Wofsy (1974) derives a somewhat drier cloud model with its bottom near 50 km, while microwave data imply a cloud mass intermediate between these models (Rossow and Sagan, 1975). The results of the Venera photometer experiment can be interpreted in terms of a cloud bottom between 30 and 35 km altitude (Marov *et al.*, 1973). Since all of these altitudes are within one scale height of each other, we adopt 32 km as the altitude of the pyrolysis level. (Some earlier calculations were performed with a pyrolysis level at 36 km.)

The condensation (or evaporation) time constant for a sulfuric acid droplet can be estimated from the time required by a droplet to e-fold its mass (Mason, 1971), i.e.,

$$\tau_{\rm cond}^{-1}=\frac{3\rho_s S}{\rho_c}a^{-2}D, \quad (7)$$

where ρ_s is the saturation vapor density, S the supersaturation (or undersaturation) of the vapor, ρ_c the density of the condensed phase, a the droplet radius, and D is the diffusion coefficient which is inversely proportional to the atmospheric density. Assuming a value of $S\gtrsim 1\%$, a saturation vapor pressure $\sim 10^{-5}\rho$ (approximately the mass mixing ratio of sulfuric acid) and a droplet size of ~ 1 μm, we have $\tau_{\rm cond}\lesssim 10^3$ s.

The coagulation time constant is given by (Fuchs, 1964)

$$\tau_{\rm coag}^{-1}=\frac{4kT}{3\eta}n, \quad (8)$$

where η is the dynamic viscosity of the atmosphere. For a droplet number density near the cloud tops, $n\sim 10^3$ cm^{-3} (Samuelson *et al.*, 1975), $\tau_{\rm coag}\sim 10^7$ s. The sedimentation time constant for 1 μm droplets throughout the cloud is $\tau_{\rm fall}\sim H/V_s\sim 3\times 10^7$ s, where H is the gas scale height, while the eddy mixing time constant is $\tau_{\rm eddy}\sim H^2/E$.

Thus, as long as the droplet number density is $\lesssim 10^7$ cm^{-3} and the eddy diffusivity $\lesssim 10^8$ cm^2 s^{-1}, condensation or evaporation is more rapid than any other process near the cloud bottom. Since evaporation is so rapid and the equilibrium vapor pressure of sulfuric acid over the droplets is such a strong

function of temperature (i.e., altitude), droplets reaching the pyrolysis level are almost instantly destroyed. Therefore we model evaporation at the cloud bottom by setting the droplet number density at the pyrolysis level equal to zero.

The fate of the sulfuric acid vapor in the lower Venus atmosphere depends on the atmospheric composition. If the lower atmosphere is reducing, as proposed by Lewis (1968, 1970), then gas phase reactions could destroy sulfuric acid to oxidize the reduced compounds. Prinn (1973) specifically proposes the oxidation of carbon monoxide to carbon dioxide and the formation of carbonyl sulfide. If, however, the lower atmosphere is oxidizing, as proposed by Walker (1975), then sulfuric acid would be stable in the lower atmosphere. Carbon monoxide has been detected in the upper atmosphere of Venus in amounts consistent with Lewis' (1970) model, but photochemical reactions involving carbon monoxide may account for its observed abundance (McElroy *et al.*, 1973). We have no definitive evidence about the composition of the lower atmosphere. Therefore we consider two extreme cases: 1) the lower atmosphere is reducing and the gas phase reactions are sufficiently rapid to irreversibly destroy all of the sulfuric acid below the clouds, and 2) the lower atmosphere is oxidizing and sulfuric acid is completely stable below the clouds.

In Model I the dust grains act as nucleation sites for the formation of cloud droplets. With the evaporation of the droplets at the pyrolysis level we expect to find the dust grains left behind. If the dust particles are not broken apart or combined while in the droplets, then the dust number flux across the bottom of the cloud must equal the specified dust flux at the top of the atmosphere. If no significant coagulation of the dust entering the formation layer has occurred, then the dust left behind at the pyrolysis level is 0.1 μm in radius. Therefore, for simplicity, we assume that the net downward dust flux into the pyrolysis level is equal to the net downward flux at the top of the atmosphere at the same uniform size. We show later that this assumption has no significant effect on our conclusions.

c. *Droplet formation level* (FL)

The two models of what occurs at the pyrolysis level lead to two models of the formation of the cloud droplets: 1) photochemical formation of sulfuric acid near the cloud top and 2) recondensation of sulfuric acid droplets near the cloud bottom. We model droplet condensation by specifying the mass formation rate per unit volume $S(m,z)$. For Model I clouds, the number of dust grains entering the formation level determines the number of new droplets created while in Model II clouds, the number of new droplets is specified. The specified number of droplets, together with the mass formation rate, determines the initial droplet radius. We assume all of the droplets are the same size.

The same arguments about evaporation apply to condensation near the cloud bottom. Therefore, we assume that condensation occurs entirely in the lowest layer of the cloud above the pyrolysis level.

For the photochemical model, the formation level is taken to be the line formation level at 62 km (Young, 1973). The formation region for this model is also assumed to have a small vertical extent because a consistent model of the particle growth and the structure of the upper cloud layers requires rapid conversion of vapor to particles. As discussed in the next section, the observed vertical cloud structure implies a source of particles at the bottom of or below the observed levels. Since the supply rate of vapor from below is approximately equal to the particle removal rate (or less than, in a weak mixing case), the size of the cloud particles is determined by $\tau_{\text{cond}} \approx \tau_{\text{removal}}$. For 1 μm particles in steady state at 60 km with $\tau_{\text{removal}} \sim 10^6$–$10^7$ s, the vapor density of sulfuric acid must be $\gtrsim 10\%$ of the equilibrium value [$\sim 4 \times 10^{-15}$ g cm^{-3} (Hamill *et al.*, 1977)]. This very low vapor density, $\sim 10^{-6}$ lower than the cloud density, together with the deep location of the particle source implies that the upwelling vapor is rapidly converted to particles as soon as it encounters sufficient sunlight.

For Model I clouds, the dust density at the formation level is set to zero to maximize the efficiency of the dust as condensation nuclei.

d. *Planetary surface*

The surface boundary condition applies only to the dust particles since there are no cloud droplets below the pyrolysis level. The deposition of dust onto the planetary surface is assumed to occur by turbulent deposition. The boundary condition from Paper I is

$$F_\nu(\text{surface}) = \rho V' \chi_\nu(\text{surface}), \tag{9}$$

where F_ν(surface) is given by the left-hand side of Eq. (6) evaluated at the surface and V' is the turbulent velocity near the ground taken to be $\sim U_*$, the friction velocity. For most of the results presented here, $V' = 1$ cm s^{-1}, but cases with $V' = 10$ cm s^{-1} and $V' = V_s$ are also considered. Paper I discusses the approximation required for the case $V' = V_s$.

e. *Summary of boundary conditions*

Model I calculations involve three distinct clouds: 1) a dust cloud from the droplet formation level to the top of the atmosphere, 2) a dust cloud from the planetary surface to the droplet formation level and 3) a droplet cloud above the droplet pyrolysis level. The first cloud has a specified flux as its top boundary condition and a specified density (zero) as its bottom

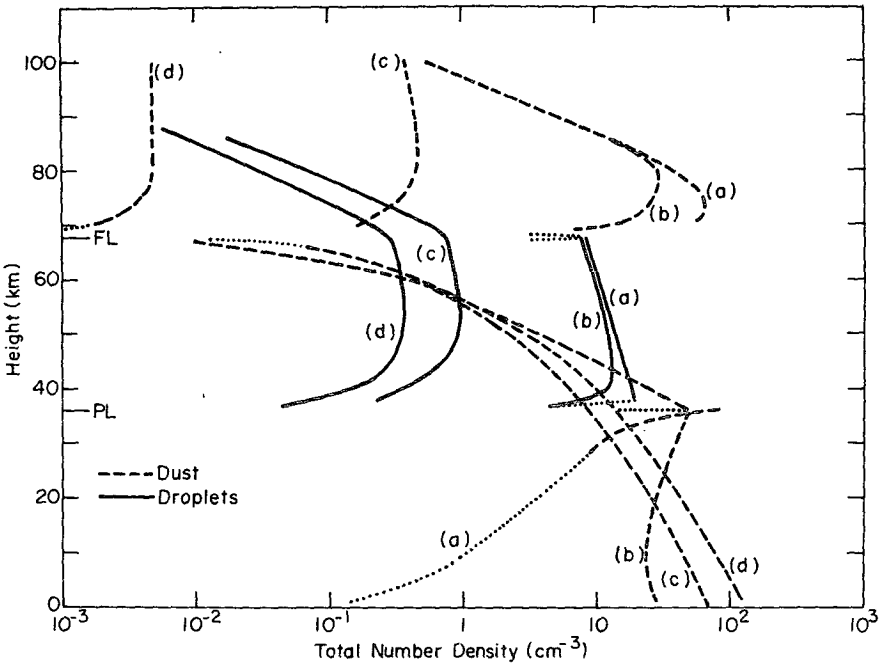

FIG. 1. Total number density as a function of altitude for dust grains and droplets for varying eddy diffusivities: (a) 10^2 cm^2 s^{-1}, (b) 10^4 cm^2 s^{-1}, (c) 10^6 cm^2 s^{-1} and (d) 10^8 cm^2 s^{-1}. The location of the formation level (FL) and the pyrolysis level (PL) is indicated.

boundary condition. The second cloud has a specified density (zero) as its top boundary condition and a surface deposition bottom boundary condition with a source of dust at the droplet pyrolysis level. These two clouds do not interact since there is no transport of dust across the droplet formation level. The third cloud has a zero flux top boundary condition and a specified density (zero) as its bottom boundary condition with a source in between at the droplet formation level. Model II calculations involve only the droplet cloud.

3. General behavior of the solutions

a. General shape of cloud vertical profile

Paper I illustrates and discusses the behavior of a single population of particles, with a source at the top of the atmosphere and a sink at the surface, influenced by coagulation, sedimentation and turbulent mixing. There are three cases: 1) the sedimentation rate is faster than either the mixing or coagulation rate (Fig. 1a, upper and middle cloud), 2) the mixing rate is faster than either the sedimentation or coagulation rate (Fig. 1d, middle cloud) and 3) the coagulation rate is equal to the transport rate producing steeper vertical gradients (Figs. 1a and 1d, lower cloud).

Since the droplets are assumed created "instantaneously," the number density at the formation level remains very much larger than the number density set by strong coagulation at all other levels. This produces such a sharp gradient in the droplet mixing ratio that mixing transport must predominate in the narrow region near the droplet formation level. Since the finite difference scheme used to solve Eq. (2) cannot handle such large gradients in the solution, we are forced, in strong coagulation cases, to choose values of the eddy diffusivity $E \gtrsim 10^4$ cm^2 s^{-1} in order to obtain a stable solution.

For a cloud or region of a cloud above a source of particles (a case not discussed in Paper I), the solutions have an important property: the maximum vertical gradient of the mixing ratio is zero. (The gradient is always negative for net upward transport.) When the net upward flux is zero, the mixing ratio is given by a balance between upward mixing and downward sedimentation, i.e.,

$$\rho E \frac{\partial q}{\partial z} = -\rho V_s q. \tag{10}$$

The solution, assuming V_s is constant, is

$$q = q_0 \exp\left[-\left(\frac{V_s H}{E}\right)\frac{z}{H}\right], \tag{11}$$

where q_0 is the mixing ratio at the source and H the gas scale height. When $V_s H/E \gg 1$, the mixing ratio decreases with altitude much more rapidly than the atmospheric density. When $V_s H/E \ll 1$, the mixing ratio is nearly constant with altitude. When the net upward flux is not zero, the most rapid transport is

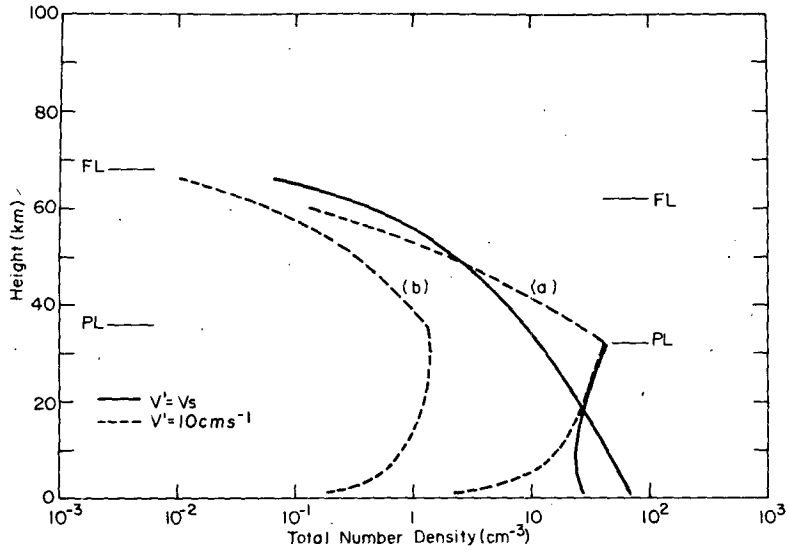

FIG. 2. Total dust number density as a function of altitude below the formation level for two eddy diffusivities [(a) 10^4 cm^2 s^{-1} and (b) 10^6 cm^2 s^{-1}] and two values of the deposition velocity.

by the strongest mixing. In this case, neglecting sedimentation, we have

$$\rho E\frac{\partial q}{\partial z}=-F, \tag{12}$$

$$q=q_0-\frac{FH}{E}\left(\frac{1}{\rho}-\frac{1}{\rho_0}\right), \tag{13}$$

where, as before, $\rho=\rho_0\exp(-z/H)$. We can see that for large E, $q\approx q_0$ until very near the top where $q\to 0$ as ρ^{-1}; for small E, q goes rapidly to zero. This behavior is illustrated by the droplet cloud above the formation level, and the dust cloud above the pyrolysis level in Fig. 1.

Comparing the general shape of the cloud vertical profiles discussed above with the observed vertical profile of the uppermost layers of the Venus clouds (O'Leary, 1975; Lacis, 1975) which has a number mixing ratio decreasing with altitude, we can rule out any cloud model with a source of droplets above the observed levels, since all such models have a number mixing ratio constant or increasing with altitude.

b. Effect of V' on the dust vertical profile

The value of V' determines the transport rate of dust grains from the droplet pyrolysis level to the surface of Venus. The effect on the dust vertical profile of changing from a very low value ($V'=V_s$) to a very high value ($V'=10$ cm s^{-1}) is illustrated in Fig. 2 for a weak and strong mixing case. Even though V' changes by approximately four orders of magnitude, the dust density near the cloud bottom changes by only one order of magnitude for the strong mixing case. Thus the dust density at and above the droplet pyrolysis level is not a very sensitive function of our choice of V'.

c. Effect of E on the vertical profile

For clouds with a source of droplets near the top and a sink for droplets at the bottom, the net transport is downward. The number density of cloud particles is then given by the supply rate divided by the transport rate. Therefore the maximum cloud density occurs for the slowest transport rate, which is the sedimentation rate. Turbulent mixing only serves to increase the transport rate and decrease the cloud density. This conclusion holds for strongly coagulating clouds as well.

When the source of droplets is near the bottom of the cloud, the largest cloud density above the source occurs when the mixing is strong above the source. In this case, increasing the mixing increases the density of the cloud until a nearly constant mixing ratio is attained. A further increase of the mixing has little effect. The dust cloud above the pyrolysis level is supplied from a source whose strength is a function of the mixing; thus its behavior is more complex. Increased mixing serves to redistribute the mass in this layer rather than to increase the total mass. Therefore, the increase of the droplet cloud density caused by an increased dust supply from the pyrolysis level is less sensitive to increased mixing than the decrease of the droplet cloud density caused by increased transport to the pyrolysis level. This is shown by comparing Figs. 1b, 1c and 1d.

We consider two cases for the variation of the eddy diffusivity with altitude. The simplest case assumes

that E is constant throughout the atmosphere. This assumption is almost certainly unrealistic, but allows us to investigate the behavior of the droplet clouds for a simple case. On the other hand, if the eddy motions are thermally driven, it is possible that mixing is strong within the cloud, where radiation is primarily absorbed and emitted. Therefore, we also investigate cases with weak mixing above and below the cloud layer and strong mixing within the cloud layer.

4. Results and discussion

The numerical method used to solve Eq. (2) is described in Paper I. The dust and droplets in Model I calculations are treated as separate populations coupled by the boundary conditions at the droplet formation and pyrolysis levels. An additional sink for dust above the pyrolysis level is coagulation with cloud droplets, but this was found to be a small effect. We assume for simplicity that coagulation destroys the dust grains while adding negligible mass to the droplet. The model atmosphere is taken from Marov (1972).

We consider five distinct cases:

Model I

(i) The droplet formation level is at or near 62 km and the eddy diffusivity is assumed constant throughout the atmosphere.
(ii) The droplet formation level is at or near 62 km and the eddy diffusivity is larger in the cloud layer.
(iii) The droplet formation level is at 33 km.

Model II

(i) The droplet formation level is at 62 km and the eddy diffusivity is larger in the cloud layer.
(ii) The droplet formation level is at 33 km and the eddy diffusivity is constant throughout the atmosphere.

a. Model I

(i) We use this case to investigate the influence on the cloud structure not only of the meteoritic dust but also of the dust supplied to the formation level from below. In the calculations presented here this source of dust is at the pyrolysis level. We maximize the upward dust flux by choosing $V'=V_s$ to minimize downward transport of dust and by choosing a large, constant eddy diffusivity to maximize the upward transport. The sequence of cloud profiles in Fig. 1 illustrates that increased mixing fails to increase the cloud density over that given by sedimentation. Thus dust from the pyrolysis level cannot increase the cloud density over that produced by the meteoritic dust alone falling into the formation level from above.

Turning to the maximum mass clouds, which are the two sedimentation-dominated cases (Figs. 1a and 1b), we find that the mass mixing ratio of these clouds at the top is $\sim 10^{-7}$, which is much smaller than the derived mass mixing ratios of Samuelson *et al.* (1975), Belton *et al.* (1968), Regas *et al.* (1972, 1975) and Hansen and Hovenier (1974) for these regions. (In order to match the observed vertical profile in the upper layers, we must assume slightly stronger mixing above the formation level.) For 1 μm droplets, this corresponds, in both cases, to a droplet number density near the cloud top of ~ 10 cm^{-3}. Thus a meteoritic dust flux of ~ 1 cm^2 s^{-1} fails to produce sufficient number density in the cloud to match observations.

Fig. 3 illustrates the important result that the dust number density in the lower atmosphere is limited by coagulation. This can be understood by equating a mixing time of $\sim H^2/E$ to the coagulation time, giving

$$n \approx \frac{\eta E}{kTH^2}. \tag{14}$$

For $E=10^6$ cm^2 s^{-1} as in Fig. 3, $n \sim 10^3$ cm^{-3} at the surface. Thus, coagulation serves to limit the maximum density of a potential source of dust at the surface of the planet. Since the droplet formation level is approximately five or six scale heights above the surface, the dust number density at this level (which can be converted to a droplet number density) is more than two orders of magnitude smaller than the surface number density. Even if very strong mixing could produce a dust number density at the droplet formation level of the right magnitude, this same strong mixing transports the droplets so rapidly to the pyrolysis level that the cloud density again falls well below observed values. Therefore, we conclude that a potential source of nucleation centers at the surface also fails to account for the observed cloud number density.

(ii) We attempt to maximize the effect of the meteoritic dust flux from above by assuming an eddy diffusivity which varies with altitude. Fig. 4 shows a sequence of cloud profiles where the mixing is first increased in the whole atmosphere and then decreased below the cloud. The important result is that the cloud density never exceeds that of the weak mixing cloud (Fig. 4a). If we further decrease the transport to the pyrolysis level by moving the lower "kink" in the eddy diffusivity profile to a higher altitude, this only serves to redistribute the density in cloud c, increasing the density at the bottom at the expense of the density at the top. Thus stronger mixing within the cloud cannot increase the cloud density. Note that, even though the assumed meteoritic dust flux here is 10^2 cm^{-2} s^{-1}, these clouds also fail to attain

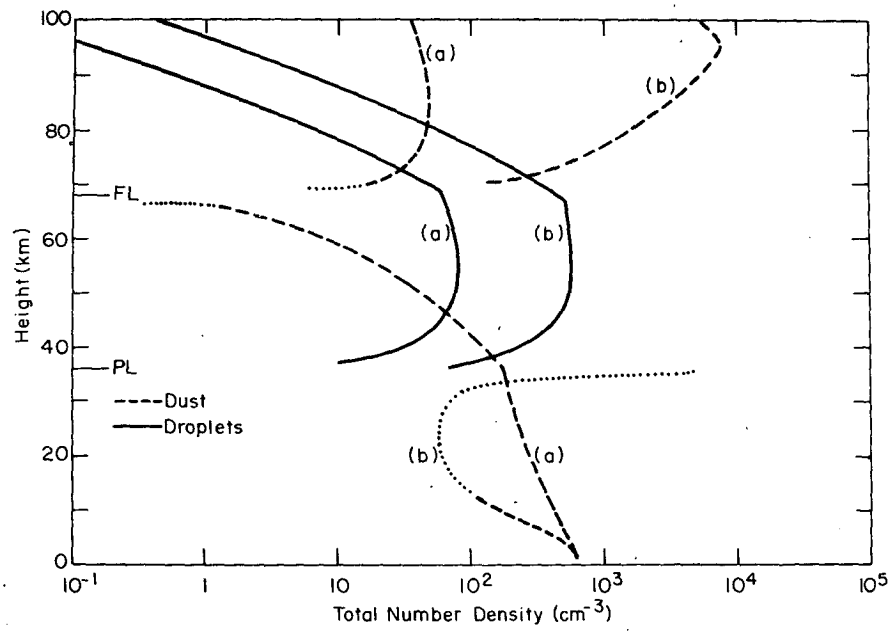

FIG. 3. Total number density as a function of altitude for dust grains and droplets for two values of the meteoritic dust flux: (a) 10^2 cm^{-2} s^{-1} and (b) 10^4 cm^{-2} s^{-1}.

the observed number density by almost an order of magnitude.

(iii) We investigate one final model with the droplet formation level at the bottom of the cloud. The maximum droplet number density at the cloud top for a given number density at the cloud bottom is produced by strong mixing in the cloud which leads to a number density proportional to the atmospheric density. Thus, even though the formation level is now two to three scale heights closer to a potential source of dust at the surface, the fact that the cloud top is two to three scale heights still higher results in a low number density. This model also fails to account for the observed droplet number density.

Thus we conclude from Model I results that a meteoritic flux of 1 cm^{-2} s^{-1} fails to account for the observed cloud number density even if we assume that the dust grains are 100% efficient as nucleation

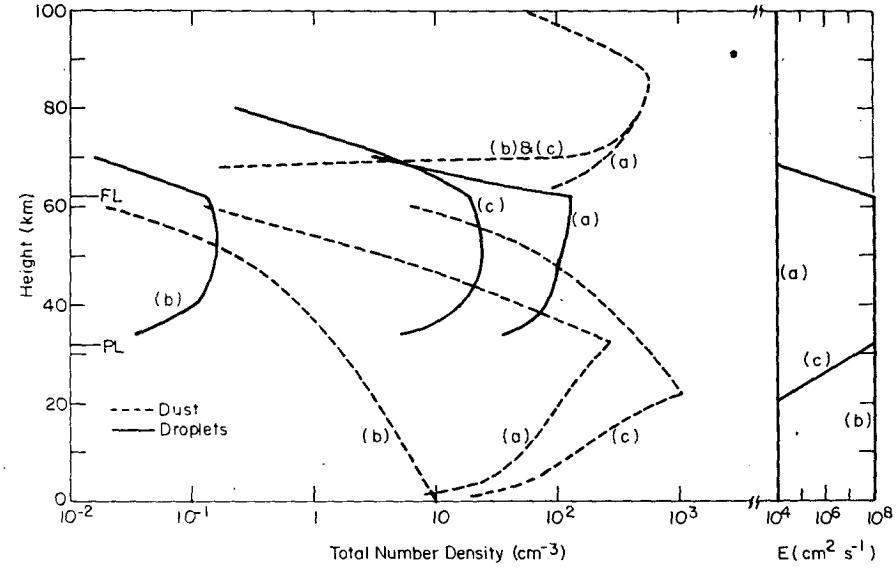

FIG. 4. Total number density as a function of altitude for dust grains and droplets for three different eddy diffusivity variations with altitude: (a) constant, (b) high below FL, and (c) high only in cloud layer.

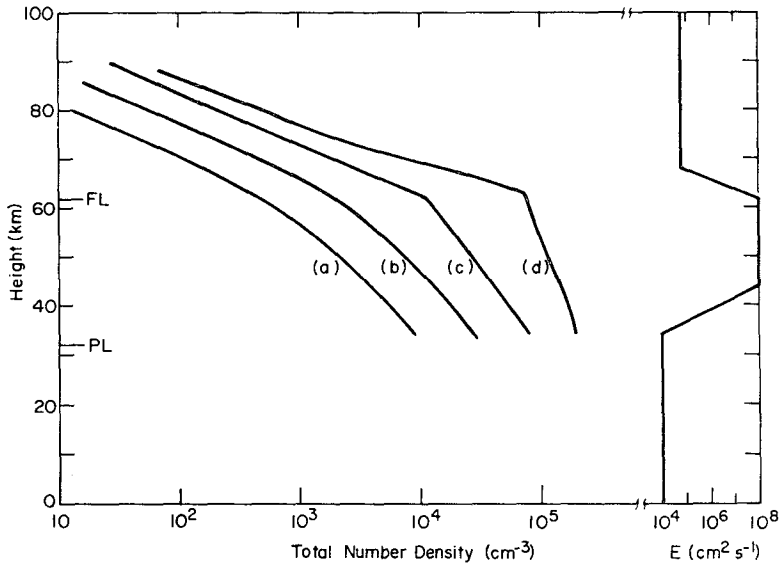

FIG. 5. Total droplet number density as a function of altitude for four values of the cloud mass creation rate: (a) 4×10^{-16} g cm^{-3} s^{-1}, (b) 4×10^{-15} g cm^{-3} s^{-1}, (c) 4×10^{-14} g cm^{-3} s^{-1} and (d) 4×10^{-13} g cm^{-3} s^{-1}.

centers. The clouds which do result are so sparse that no significant coagulation occurs. The meteoritic dust flux required to produce the observed cloud density is approximately three orders of magnitude greater than the flux into Earth's atmosphere. A source of 0.1 μm dust or larger meteorites (to produce ablation products) many orders of magnitude greater than near the Earth is inconsistent with observations (Dohnanyi, 1972).

b. Model II

(i) We examine cases which have the observed cloud density. We optimize conditions for strong coagulation by assuming weak mixing near the pyrolysis level to maximize the lifetime of a droplet in the cloud and by assuming strong mixing through the remainder of the cloud in order to rapidly remove the initial droplet sizes from observed levels and to replace them with sizes created by coagulation which is most rapid near the cloud bottom. If mixing throughout the cloud is weak, then the larger droplets created by coagulation are not brought up to observable levels. Therefore we choose the eddy diffusivity $E=10^8$ cm^2 s^{-1} throughout the bulk of the cloud with weaker mixing $E=10^4$ cm^2 s^{-1} near the pyrolysis level. For droplets with radii $\gtrsim 1$ μm, this insures transport by sedimentation at these levels. We also assume weaker mixing above the formation level, i.e., $E=7\times10^4$ cm^2 s^{-1}.

Figs. 5 and 6 illustrate results for clouds with initial droplet radii of 0.1 and 0.5 μm, respectively. Samuelson *et al.* (1975) and Rossow and Sagan (1975) together imply an upper limit to the cloud mass mixing ratio near 62 km between 5×10^{-6} and 10^{-5}. We have not performed calculations for values larger than 10^{-5}. The properties of these clouds at the droplet formation level are shown in Table 1. The mean droplet radius is the radius which gives the mean mass as defined by Eq. (5).

The evolution in the shape of the cloud profile with increasing droplet creation rate (compare Figs. 5a, 5d and 6c) is the result of the increasing mean droplet radius near the cloud bottom. Since the transport of droplets to the pyrolysis level is by sedimentation, increasing the mean droplet radius rapidly increases the transport rate to the pyrolysis level until in Fig. 6c, the solution has switched from $n\propto\rho$ behavior to $n\propto\rho^{-1}$ behavior as discussed in Section 3. This effect explains the evolution of the mean droplet radius at the formation layer exhibited in Table 1. As the droplet creation rate increases, the mean radius at 62 km is increased by the upward mixing of larger droplets created by coagulation. A further increase in the droplet creation rate, however, produces such large droplets by coagulation that they are removed by sedimentation rather than contributing to an increase of the mean radius at 62 km. Thus the cloud model with an initial droplet radius of 0.1 μm failed to attain a 1 μm mean droplet radius at 62 km.

Faster mixing at the pyrolysis level inhibits significant coagulation even for clouds with mass mixing ratios $\sim10^{-5}$ at the droplet formation level. Therefore, we conclude that cloud models with the droplet formation level near the top (photochemical model) can only produce, at most, a factor of 2 or 3 increase in the mean droplet radius by coagulation. This is a general consequence of the formation level being so close to the observed levels that the initial size dis-

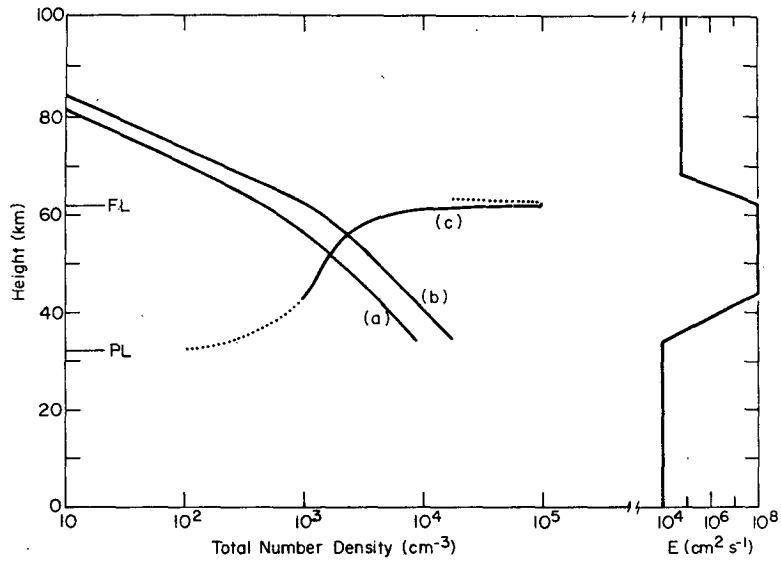

FIG. 6. Total droplet number density as a function of altitude for three values of the cloud mass creation rate: (a) 5×10^{-14} g cm^{-3} s^{-1}, (b) 2×10^{-13} g cm^{-3} s^{-1} and (c) 5×10^{-12} g cm^{-3} s^{-1}.

tribution predominates at these levels. Thus, to account for 1 μm droplets we must assume for the photochemical model, that the initial droplet radius is $\gtrsim 0.5$ μm.

Hansen and Hovenier (1974) not only derived from the polarization observations a mean droplet radius, defined by

$$r_e=\left[\int_0^\infty r^3n(r)dr\right]\Big/\left[\int_0^\infty r^2n(r)dr\right], \qquad (15)$$

where $r_e=1.05\pm0.1$ μm, but also the variance of the size distribution defined by

$$v_e+1=\left[\int_0^\infty r^4n(r)dr\right]\left[\int_0^\infty r^2n(r)dr\right]\Big/\left[\int_0^\infty r^3n(r)dr\right]^2, \qquad (16)$$

TABLE 1. Properties of photochemical cloud model at droplet formation level.

Curve label	Droplet creation rate (cm^{-3} s^{-1})	Initial droplet radius (μm)	Mean droplet radius (μm)	Variance	Mass mixing ratio
8a	10^{-1}	0.1	0.25	44	9.1×10^{-8}
8b	1	0.1	0.30	190	6.5×10^{-7}
8c	10	0.1	0.30	1000	3.3×10^{-6}
8d	10^2	0.1	0.24	8200	1.2×10^{-5}
9a	10^{-1}	0.5	0.99	32	5.5×10^{-6}
9b	4×10^{-1}	0.5	1.0	66	1.4×10^{-5}
9c	10	0.5	0.80	380	1.4×10^{-3}

where $v_e=0.07\pm1.02$. In our calculations, we derive a mean radius defined by

$$\bar{r}=\left[\int_0^\infty r^3n(r)dr\right]^{\frac{1}{3}}\Big/\left[\int_0^\infty n(r)dr\right]^{\frac{1}{3}} \qquad (17)$$

and a variance of the size distribution defined by

$$\sigma^2+1=\left[\int_0^\infty r^6n(r)dr\right]\left[\int_0^\infty n(r)dr\right]\Big/\left[\int_0^\infty r^3n(r)dr\right]^2. \qquad (18)$$

Using the same size distribution function as Hansen and Hovenier (1974), we derive the relations

$$\bar{r}=[(1-v_e)(1-2v_e)]^{\frac{1}{3}}r_e, \qquad (19)$$

$$\sigma^2=3\left[\frac{2v_e^2+3v_e+3}{2v_e^2-3v_e+1}\right]v_e. \qquad (20)$$

These expressions are physically meaningful only when $v_e<0.5$, since the bottom integral in (17) has a singularity at $v_e=0.5$. However, since the choice of the size distribution function is only a matter of convenience, Eqs. (19) and (20) are not fundamental in any sense, so we use the qualitative relations derivable from (19) and (20), i.e., $\bar{r}\approx r_e$ and $\sigma^2\approx10\ v_e$. The results are approximately the same for other functions. The order of magnitude of σ^2 is sufficient to choose between the results of the models; that is, our conclusions are not sensitive to the precise values of $\bar{r}$ and σ^2.

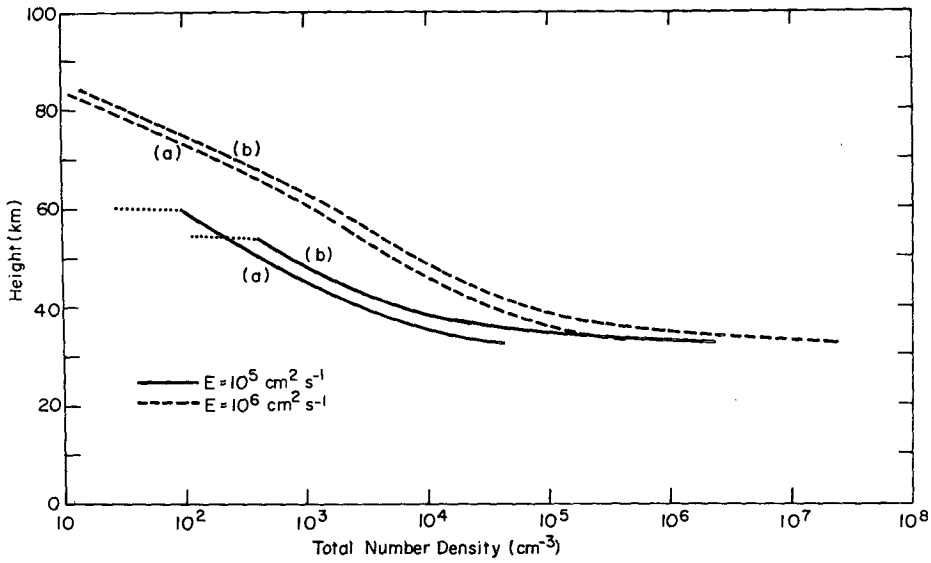

FIG. 7. Total droplet number density as a function of altitude for two values of the eddy diffusivity [10^5 cm^2 s^{-1} and 10^6 cm^2 s^{-1}] and two values of the initial droplet radius [(a) 0.5 μm and (b) 0.05 μm].

Since the photochemical cloud model can only produce a twofold or threefold increase in the mean droplet radius by coagulation, the initial droplets are larger than the shortest wavelengths analyzed by Hansen and Hovenier and cannot escape detection. The large variance ($\sim 10^2$) for these cloud models is thus inconsistent with their results. Since the absorption of long wavelength radiation is independent of droplet radii, the mass determinations of these clouds include the mass of any population of smaller droplets; whereas, droplets with radii much smaller than the wavelengths of the polarization observations are not effective scatterers and would escape detection. Thus the upper limit on the mass mixing ratio is firm. If the photochemical model is correct, then the observed droplet size distribution is the initial size distribution with little ($<50\%$) increase of the mean droplet radius by coagulation. Droplets of nearly 1 μm radius must be produced directly by photochemistry and condensation in order to match the observations.

If coagulation is to be negligible in these clouds then either the cloud mass mixing ratio is smaller than 10^{-6}, reducing the coagulation rate, or the transport rate near the pyrolysis level is higher than the sedimentation rate, reducing the lifetime of a droplet in the cloud. Figs. 5a and 6a suggest that the droplet

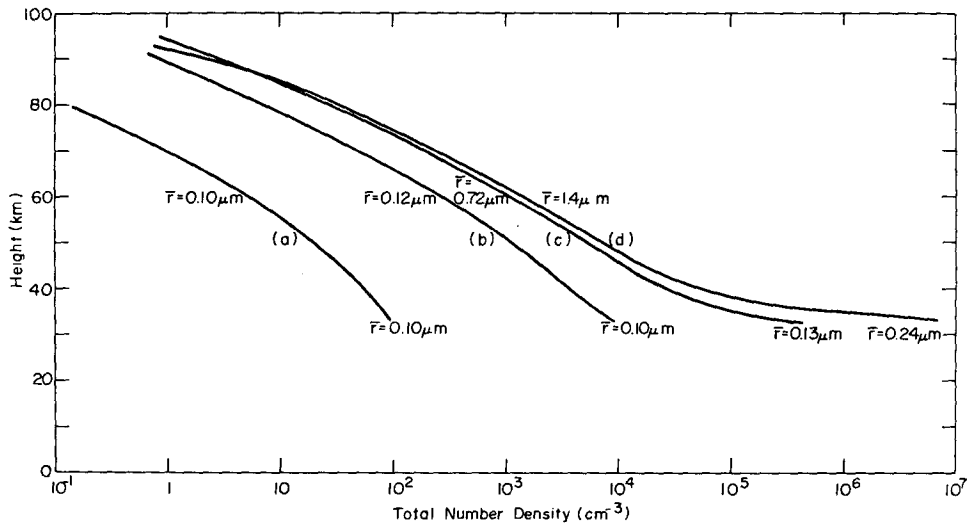

FIG. 8. Total droplet number density as a function of altitude for four values of the cloud mass creation rate: (a) 4×10^{-17} g cm^{-3} s^{-1}, (b) 4×10^{-15} g cm^{-3} s^{-1}, (c) 4×10^{-13} g cm^{-3} s^{-1} and (d) 4×10^{-11} g cm^{-3} s^{-1}.

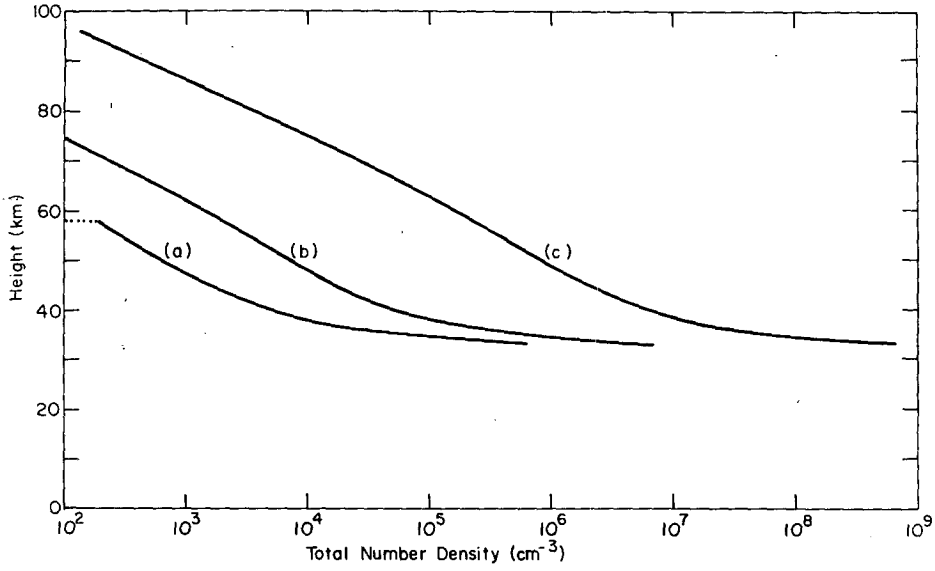

FIG. 9. Total droplet number density as a function of altitude for three values of the eddy diffusivity: (a) 10^5 cm^2 s^{-1}, (b) 10^6 cm^2 s^{-1} and (c) 10^8 cm^2 s^{-1}.

number density near the droplet formation level must be less than 10^2 cm^{-3} in order to inhibit coagulation, but this value is only barely consistent with some observations (Belton *et al.*, 1968). If the number density near the formation level is $\sim 10^3$ cm^{-3}, then the lifetime of a droplet in the cloud must be less than the coagulation time in order to prevent significant coagulation. For $n \sim 10^3$ cm^{-3}, $\tau_{coag} \sim 10^7$ s. For faster transport to the pyrolysis level, the cloud number density is roughly constant with altitude. The droplet residence time is then given by the column number density ($\sim nD$), where D is the depth of the cloud layer, divided by the flux of droplets to the pyrolysis level ($\sim nE/H$). Then

$$\tau_{res} \sim DH/E < \tau_{coag} \sim 10^7 \text{ s}$$

implies $E > 3 \times 10^5$ cm^2 s^{-1} and a cloud mass flux $> 10^{-9}$ gm cm^{-2} s^{-1}.

(ii) The photochemical cloud model is unable to produce a narrow, coagulation-dominated size distribution primarily because the droplet formation level is near the observed levels and the rapidly forming droplets dominate the size distribution. The recondensation cloud model places the droplet formation level at the bottom of the cloud (at 33 km), several scale heights below the observed levels. The solution in this case involves a balance between upward mixing transport and downward sedimentation, with coagulation acting as a sink at all levels. For simplicity we consider only a constant eddy diffusivity.

TABLE 2. Properties of recondensation cloud model at 62 km level.

Droplet creation rate (cm^{-3} s^{-1})	Initial droplet radius (μm)	Mean droplet radius (μm)	Variance	Mass mixing ratio
10^2	0.5	1.7	4.1	4.6×10^{-5}
10^4	0.1	1.4	6.0	3.7×10^{-5}
10^5	0.05	1.4	6.8	4.4×10^{-5}
10^7	0.01	1.3	7.3	3.6×10^{-5}

The results are displayed in Figs. 7, 8 and 9. Fig. 7 shows that the eddy diffusivity must be $> 10^5$ cm^2 s^{-1} in order to mix 1 μm droplets upward to the observed levels. This result is independent of the assumed initial droplet size. Fig. 8 illustrates the effect of coagulation on the solution. For $E = 10^6$ cm^2 s^{-1}, the number density throughout the cloud is limited by the balance between coagulation and transport rates. Further increase of the droplet creation rate only increases the resulting mean droplet size $\bar{r}$. If we adjust the droplet creation rate to give a mean droplet radius of 1 μm at 62 km, then Fig. 9 demonstrates that the eddy diffusivity must be between 10^5 and 10^6 cm^2 s^{-1} in order to obtain a mass mixing ratio $\sim 10^{-5}$ in coagulation-limited clouds.

The most important property of these results is shown in Table 2 which indicates that for these coagulation-limited clouds, the mean droplet radius at 62 km reaches micron size independently of the assumed initial droplet radius. All of these results together imply that since the number density of the droplets is a function only of the eddy diffusivity, the resulting mean droplet radius is determined only by the assumed mass creation rate, which is $\sim 5 \times 10^{-11}$ gm cm^{-3} s^{-1} for all of the cases in Table 2.

The variance of the size distribution is a function of the initial droplet radius as Table 2 shows, growing

larger as the initial radius decreases. However, unlike the photochemical cloud model, the initial droplets can now be much smaller than the shortest wavelengths analyzed by Hansen and Hovenier (1974) and therefore may escape detection. The effective variance may then be smaller than indicated in Table 2. We note that the variance of a coagulation-dominated size distribution as calculated by Friedlander and Wang (1966) is unity, which is consistent with Hansen and Hovenier's results.

5. Summary and conclusions

The calculations presented here are an attempt to understand whether the observed size distribution in the upper regions of the Venus clouds is a direct consequence of the condensation process or is produced by an interaction of coagulation and dynamics. That is, since the only modification of a size distribution produced by turbulent mixing and sedimentation is the removal of the larger droplets, the observed mean droplet radius and narrow size distribution could be determined solely by the minimum radius in the originally formed size distribution. On the other hand, the observed size distribution could be determined by the interaction of coagulation and dynamics independent of the initial size distribution. Our conclusions, therefore, fall into two categories: 1) the conditions present in the clouds necessary to prevent significant modification of the initial droplet size distribution by coagulation, and 2) the conditions which produce the observed size distribution by the interaction of coagulation and dynamics.

Since we have underestimated the coagulation coefficient at these altitudes somewhat (Hidy and Brock, 1965), a number density as high as 10^3 cm^{-3} implies that coagulation will occur at the observable levels unless the turbulent mixing is sufficiently rapid. Mixing represented by $E>10^6$ cm^2 s^{-1} is required throughout the whole cloud layer. The mixing ratio resulting from an eddy diffusivity this large is approximately proportional to $(\rho^{-1}-\rho_0^{-1})$ which implies a number density nearly constant with altitude between the droplet formation level and the pyrolysis level. Strong mixing also implies negligible modification of the size distribution by sedimentation.

When coagulation is insignificant, condensation must determine both the number and the size of the droplets present in the clouds. One simple model for the influence of dynamic motions on the formation of droplets is that the dynamics control the supply of nucleation centers upon which the droplets form. Since the coagulation rate for the smaller condensation nuclei is roughly equal to or less than that for the same number density of droplets (Hidy and Brock, 1965), the number density of condensation nuclei is not strongly controlled by coagulation either. We have investigated two sources of supply for these nucleation centers, meteoritic dust and surface dust, and find that neither supply is adequate to explain the observed cloud droplet number density. Thus, the number density of the droplets is not controlled by the number of available nucleation centers unless some more prolific source is found.

One consequence of this investigation is that the number density of dust grains near the surface of Venus is limited by coagulation. The limiting number density is given by a balance between the coagulation and transport rates as given in Eq. (14), e.g., if $E=10^6$ cm^2 s^{-1}, then $n\lesssim 10^3$ cm^{-3}.

Significant coagulation in a photochemical cloud model can only produce a factor of 2 or 3 increase in the mean droplet radius but in so doing produces a variance at least in order of magnitude too large to be consistent with the analysis of Hansen and Hovenier (1974). Thus if the photochemical model correctly describes the location of the droplet formation level, the observations rule out significant coagulation and imply a lower limit on the eddy diffusivity $E\gtrsim 10^6$ cm^2 s^{-1} in the lower cloud layer (below $\sim$60 km) and a lower limit on the mass flux through the cloud of

$$F_{\text{mass}}\gtrsim 5\times 10^{-9}\text{ g cm}^{-2}\text{ s}^{-1}.$$

If we need one UV ($\lambda\approx 3000$ Å) photon for each molecule, this mass flux requires an efficiency factor of 10^{-3} for production of sulfuric acid molecules to account for this mass flux. The mass flux may be limited by the supply of photons available. The photochemical model also requires a prolific source of condensation nuclei.

If the droplet number density is indeed $\sim 10^3$ cm^{-3}, then significant coagulation occurs if the eddy diffusivity is $10^5<E<10^6$ cm^2 s^{-1}. In this case the droplets must be formed near the bottom of the cloud in order to be consistent with the analysis of Hansen and Hovenier (1974). The 1 μm mean droplet size is a function only of the mass creation rate per unit volume, which is proportional to the mass mixing ratio of vapor below the cloud, and the number density is a function only of the eddy diffusivity in these coagulation-limited clouds. All information about the initial droplet size distribution, except that the mean radius is initially $\lesssim 0.1$ μm, is lost; the details of the droplet condensation process are unimportant. The initial droplets must be $\lesssim 0.1$ μm so that they do not influence the polarization results. This cloud model also requires a very prolific source of condensation nuclei in order to produce initial droplets $\lesssim 0.1$ μm in radius.

In a comparison of the solutions of Eq. (1) obtained by the approximate technique used here and by a more accurate discrete size distribution calculation (Paper I), we find that the approximations employed result primarily in inaccurate values of the third moment of the size distribution. The accuracy of this

technique is highest for strong mixing cases, since it is the sedimentation term which requires approximation. Thus we expect our results to be quite accurate for all cases with mixing stronger than $\sim 10^5$ cm^2 s^{-1} for 1 μm droplets. Since we were able to discount most of the weak mixing cases on qualitative grounds, our conclusions based on this approximate technique are firm.

On the basis of the results presented here, we cannot choose between the two cloud models that are consistent with the polarization results of Hansen and Hovenier (1974): a photochemical model in which the droplet size is determined by the balance between the condensation growth time and the lifetime of a droplet in the formation region and a stable vapor model in which the number density of the droplets is determined by the balance between the coagulation growth time and the lifetime of the droplets in the cloud. The unsatisfactory feature of the first model is that the mechanism which determines the number density of the droplets is not specified. Comparing the photochemical model to an equivalent model of sulfuric acid growth in Earth's stratosphere (Hamill *et al.*, 1977), we find that the lower steady-state supersaturation required in the Venus clouds suggests that nucleation must occur on Aitken particles at these low temperatures, but only inefficiently. Condensation on ions, for example, would probably require larger supersaturations. We have shown that neither meteoritic or surface dust can supply sufficient condensation nuclei to the formation region and that, with some other more prolific source of condensation nuclei, coagulation cannot efficiently control the number density of condensation nuclei without noticeable effects on the cloud droplets.

On the other hand, the size of the droplets in the second model is determined solely by the mass density of the cloud independently of the nucleation process. However, in order to escape detection in the polarization observations the initial droplets must be quite small, again requiring the nucleation of numerous droplets. (The uncertainties in the derived values of σ^2 are sufficiently large that this requirement may not be necessary.) Comparing this model to the observed "sulfate" Aitken particles forming urban smogs in Earth's troposphere, we suggest that the nucleation of numerous, small sulfuric acid droplets by gas phase chemical reactions (Vohra and Nair, 1970) may be quite efficient at the higher temperatures at the cloud base. The uncertainties in the chemical composition of the Venus atmosphere, as well as in the theory of nucleation, are so large, however, that neither of these models can be disregarded.

Choosing between these two models observationally may prove quite difficult because of the difficulty in detecting particles of Aitken size. The photochemical (top forming) model has a nearly constant droplet number density with depth below the formation level (Fig. 1) with mean droplet radius increasing slightly (to ~ 2 μm) because of more rapid coagulation in the lower levels. The recondensation (bottom forming) model has an increasing droplet number density ($n \propto \rho$) with depth (Fig. 8), but with a decreasing mean droplet radius as we approach the formation level. Although the vertical profile of cloud droplet number density and mean size for a cloud forming near the top is very different from that for a cloud forming near the bottom, the very small mean radius of the droplets in the lower portions of the stable vapor model (Fig. 8) may make these droplets invisible to detection by optical wavelengths. Determining which of these two models best describes the clouds of Venus has important consequences for the chemistry of the lower atmosphere. In order for sulfuric acid vapor to be stable in the lower atmosphere, in contrast to the photochemical model, the atmosphere must be completely oxidized as might occur after the loss of massive amounts of water from the primeval atmosphere of Venus (Walker, 1975).

Acknowledgments. I wish to acknowledge the very helpful comments and advice of Peter J. Gierasch, Edwin E. Salpeter and Michael Belton. This work has been supported in part by NASA Grant NGL-33-010-186 and by NOAA Grant 04-3-022-33.

REFERENCES

Belton, M. J. S., D. M. Hunten and R. M. Goody, 1968: *The Atmosphere of Venus and Mars*, J. C. Brandt and M. B. McElroy, Eds. Gordon and Breach, 288 pp.

Dohnanyi, J. S., 1972: Interplanetary objects in review: Statistics of their masses and dynamics. *Icarus*, **17**, 1–48.

Friedlander, S. K., and C. S. Wang, 1966: The self-preserving particle size distribution for coagulation by Brownian motion. *J. Colloid Interface Sci.*, **22**, 126–132.

Fuchs, N. A., 1964: *The Mechanics of Aerosols*, R. E. Daisley, M. Fuchs and C. N. Davies, Eds. Pergamon Press, 408 pp.

Goody, R. M., 1967: The scale height of the Venus haze layer. *Planet. Space Sci.*, **15**, 1817–1819.

Hamill, P., O. B. Toon and C. S. Kiang, 1977: A physical model of the stratosphere aerosol particles. (Submitted to *J. Atmos. Sci.*)

Hansen, J. E., and J. W. Hovenier, 1974: Interpretation of the polarization of Venus. *J. Atmos. Sci.*, **31**, 1137–1160.

Hidy, G. M., and J. R. Brock, 1965: Some remarks about the coagulation of aerosol particles by Brownian motion. *J. Colloid Interface Sci.*, **20**, 477–491.

Ingersoll, A. P., and G. S. Orton, 1974: Lateral inhomogeneities in the Venus atmosphere: Analysis of thermal infrared maps. *Icarus*, **21**, 121–128.

Klett, J. D., and M. H. Davis, 1973: Theoretical collision efficiencies of cloud droplets at small Reynolds numbers. *J. Atmos. Sci.*, **30**, 107–117.

Lacis, A. A., 1975: Cloud structure and heating rates in the atmosphere of Venus. *J. Atmos. Sci.*, **31**, 1107–1124.

Lewis, J. S., 1968: An estimate of the surface conditions of Venus. *Icarus*, **8**, 434–456.

——, 1970: Venus: Atmospheric and lithospheric composition. *Earth Planet. Sci. Lett.*, **10**, 73–80.

Marov, M. Ya., 1972: Venus: A perspective of the beginning of planetary exploration. *Icarus*, **16**, 415–461.

——, V. S. Avduevsky, N. F. Borodin, A. P. Ekonomov, V. V. Kerzhanovich, V. P. Lysov, B. Ye. Moshkine, M. K. Rozhdestvensky and O. L. Ryabov, 1973: Preliminary results on the Venus atmosphere from Venera 8 descent module. *Icarus*, **20**, 407–421.

Mason, B. J., 1971: *The Physics of Clouds*. Clarendon Press, 671 pp.

McElroy, M. B., N. D. Sze and Y. L. Yung, 1973: Photochemistry of the Venus atmosphere. *J. Atmos. Sci.*, **30**, 1437–1447.

O'Leary, B., 1975: Venus: Vertical structure of stratospheric hazes from Mariner 10 pictures. *J. Atmos. Sci.*, **32**, 1091–1100.

Pollack, J. B., E. F. Erickson, D. Goorvitch, B. J. Baldwin, D. L. Strecker, F. C. Witteborn and G. C. Augason, 1975: A determination of the composition of the Venus clouds from aircraft observations in the near infrared. *J. Atmos. Sci.*, **32**, 1140–1150.

Prinn, R. G., 1973: Venus: Composition and structure of the visible clouds. *Science*, **182**, 1132–1135.

Regas, J. L., L. P. Giver, R. W. Boese and J. H. Miller, 1972: Theoretical interpretation of the Venus 1.05-micron CO_2 band and the Venus 0.8189-micron H_2O line. *Astrophys. J.*, **173**, 711–725.

——, ——, —— and ——, 1975: Theoretical interpretation of the 0.7820-micron CO_2 band and 0.8226-micron H_2O line on Venus. *Icarus*, **24**, 11–18.

Rossow, W. B., and C. Sagan, 1975: Microwave boundary conditions on the atmosphere and clouds of Venus. *J. Atmos. Sci.*, **32**, 1164–1176.

——, and P. J. Gierasch, 1977: The clouds of Venus: I. An approximate technique for treating the effects of coagulation, sedimentation and turbulent mixing on an aerosol. *J. Atmos. Sci.*, **34**, 405–416.

Samuelson, R. E., R. A. Hanel, L. W. Herath, V. G. Kunde and W. C. Maguire, 1975: Venus cloud properties: Infrared opacity and mass mixing ratio. *Icarus*, **25**, 49–63.

Vohra, K. G., and P. V. N. Nair, 1970: Recent thinking on the chemical formation of aerosols in the air by gas phase reactions. *Aerosol Sci.*, **1**, 127–133.

Walker, J. C. G., 1975: Evolution of the atmosphere of Venus. *J. Atmos. Sci.*, **32**, 1248–1256.

Wofsy, S., 1974: Venus cloud models. Paper presented at Conference on the Atmosphere of Venus, Goddard Institute, 15–17 October, New York, N. Y.

Young, A. T., 1973: Are the clouds of Venus sulfuric acid? *Icarus*, **18**, 564–582.

——, 1975: The clouds of Venus. *J. Atmos. Sci.*, **32**, 1125–1132.